Magnesium Technology 2011
Edited by: Wim H. Sillekens, Sean R. Agnew, Neale R. Neelameggham, and Suveen N. Mathaudhu
TMS (The Minerals, Metals & Materials Society), 2011

Magnesium Technology 2011

Deformation Mechanisms II; Formability and Forming

Session Chairs:

Paul E. Krajewski
(General Motors, USA)
Wim H. Sillekens
(TNO Science and Industry, Netherlands)

Magnesium Technology 2011
Edited by: Wim H. Sillekens, Sean R. Agnew, Neale R. Neelameggham, and Suveen N. Mathaudhu
TMS (The Minerals, Metals & Materials Society), 2011

INFLUENCE OF SOLUTE CERIUM ON THE DEFORMATION BEHAVIOR OF A Mg-0.5 wt.% Ce ALLOY

L. Jiang[1], J.J. Jonas[1] and R. Mishra[2]
[1]Department of Materials Engineering, McGill University, Montreal, QC, H3A 2B2, Canada
[2]General Motors, Research & Development Center, Warren, MI 48090, USA

Keywords: Extruded Mg alloy bar, Dynamic strain aging, Solute cerium, Heat treatment

Abstract

The effect of solute Ce was investigated on the deformation behavior of a Mg-Ce binary alloy at elevated temperature. Compression and tension tests were performed on samples taken from extruded bars of Mg-0.5 wt.% Ce. Dynamic strain aging (DSA) was observed to occur during both tension and compression testing. Under the latter conditions, the effect of DSA on increasing the flow stress was greater than that of extension twinning. The occurrence of DSA also led to a decrease in the ductility. After heat treatment, the detrimental effect of the DSA taking place during compression was reduced significantly to an extent that depended on the cooling rate employed. However, these heat treatments did not lead to appreciable improvements in the tensile ductility.

Introduction

A number of studies have pointed out that rare earth alloying additions can significantly weaken texture sharpness in Mg alloys and thereby improve formability [1-6]. Stanford et al. [7] have shown that RE elements display stronger solute/dislocation interactions than non-RE elements. In the case of solid solution alloys such as the Mg-Y [3, 8] and Mg-Gd [9] alloys, texture weakening is observed even in the absence of second phase particles. Addition of the soluble elements Y and Gd at levels of 0.05 to 0.1 at.% also approximately doubles the extrusion force and refines the grain size by 75% [9]. This indicates that the interaction between RE solutes and dislocations and boundaries is very strong in magnesium-based alloys. It has also been observed that Ce is an effective texture modifier, probably because of its large atomic radius [9] and the effect on the Ce/Mg and Mg/Mg atomic binding states [10]. The observation of dynamic strain aging (DSA) in Mg-Ce [11] and other RE-containing alloys [7, 12-14] provides additional evidence that RE elements interact with dislocations.

In extrusion, the appropriated levels of RE alloying additions not only weaken the texture but also lead to the formation of a special component (referred to as the RE texture component): <11-21> parallel to the extrusion direction [15, 16]. Some researchers have found that the nucleation of recrystallization at shear bands plays a role in the formation of the RE texture component and texture weakening [4, 17, 18]. In steel rolling, it is well known that the formation of shear bands is favored by increasing the amount of solute carbon and rolling at temperatures where dynamic strain aging (DSA) occurs, leading to flow localization. The question therefore arises whether Ce in solution can play a similar role in Mg-based materials. Studies concerning DSA in magnesium alloys have mainly been conducted by tension testing [7, 12-14]. However, serrated flow can also occur during compression [19] and torsion [20] testing. In the current work, both uniaxial tension and compression were employed to characterize the DSA effects. The effect of different cooling rates on the Ce solute content was also investigated.

Experimental

The Mg-0.5 wt.% Ce bars were provided by the GM R&D Center, Warren, MI. The billets were preheated to 400°C for 2h and extruded at 300°C and a billet speed of 10mm/s. An extrusion of 25:1 was employed. The extrudate was water quenched right after exit from the die. The tension and compression samples were machined from the as-extruded rods with their axes aligned along the extrusion direction. The tensile specimens had gage sections 30mm long and 6mm in diameter, while the compression samples had heights of 11.6mm and diameters of 7.6mm. Various heat treatments (Table I) were carried out on the as-extruded samples in an argon atmosphere and the resulting Ce solute concentrations were measured. The mechanical tests were conducted on a servo-controlled MTS machine at 200°C. Four different strain rates were investigated: 10^{-3}, 10^{-2}, 10^{-1} and $1s^{-1}$. The samples were held for 10 min at temperature prior to testing. In order to minimize oxidation, argon gas was passed through the quartz tube enclosing the specimen and grips.

The crystallographic texture was measured by means of EBSD techniques. The Ce solute content was measured using a JEOL JXA-8900L electron probe microanalyzer (EPMA). At least 20 spots were analyzed in each case so as to provide reliable data. In preparation for the EBSD measurements, specimens were polished using standard metallographic methods followed by immersion in a solution of 10 ml HNO3, 30 ml acetic acid, 40 ml H2O and 120ml ethanol for 2s. A similar polishing procedure was employed for the EPMA samples, except that no colloidal silica was used to avoid contamination.

Table I. The Ce solute contents of the specimens after different heat treatments.

	As extruded	H1	H2	H3	H4	H5
Ce solute content (wt.%)	0.146	0.087	0.095	0.077	0.083	0.160

H1: Heated at 400°C for 4hrs, then placed on wood and cooled in air (~50°C/min)
H2: Heated at 450°C for 4hrs, then placed on a steel block and cooled in air (~75°C/min)
H3: Heated at 450°C for 4hrs, then cooled at 3°C/min

H4: Heated at 450°C for 4hrs, then cooled in the furnace (~ 25 °C/min when the temperature dropped from 450 to 250C and ~10 °C/min for temperatures from 250°C to 200°C)
H5: Heated at 450°C for 4hrs, then quenched in water to room temperature (~$2.7x10^5$°C/min) the vertical direction on the micrographs.

Results and Discussion

A typical optical microstructure from a longitudinal section of an as-extruded profile is illustrated in Figure 1. The microstructure is fully recrystallized and the average grain size is 10μm. The as-extruded texture is quite weak, with the maximum intensity peak located at <11-21> parallel to the extrusion direction (i.e. at the RE component). This is consistent with the results reported by Stanford [9].

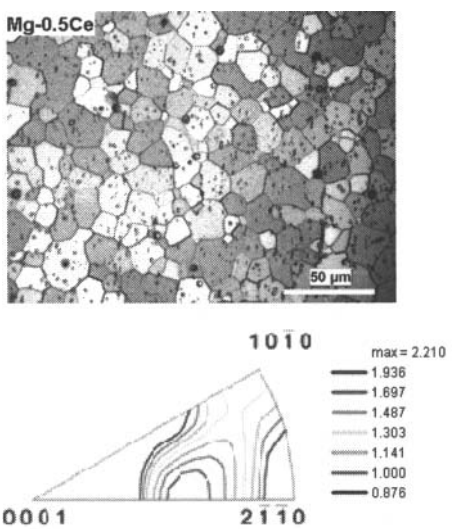

Figure 1. Microstructure and texture (presented in inverse pole figure form) of the as-extruded Mg-0.5 wt.% Ce alloy bar. The inverse pole figure refers to the extrusion direction, which is vertical in the micrograph.

The compressive true stress-strain curves determined at selected strain rates are presented in Figure 2(a). All the flow curves were sigmoidal and displayed yielding at around 70-80 MPa; this is a sign that extension twinning is taking place. Up to a strain of ~0.18, the work hardening behavior at the highest strain rate (1/s) is similar to that at the lower strain rate of 0.1/s. However, on further compression, the 0.1/s flow curve rises *above* the 1/s flow curve. It is of interest that the peak stress at the highest strain rate (1/s) is the lowest among the strain rates selected. Similar flow characteristics were observed in the 0.01/s and 0.001/s tests. The increase in strain rate produced a *decrease* in flow stress. This is indicative of a negative macroscopic strain rate sensitivity (SRS).

The corresponding tensile stress-strain curves determined under the same conditions are illustrated in Figure 2(b). When the strain rate was decreased from 0.1/s to 0.001/s, the flow stress increased and the curve displayed serrations that are symptomatic of dynamic strain aging.

Serrated flow curves (also referred to as the PLC effect) are the most commonly observed macroscopic manifestations of the DSA process. There are other anomalies associated with DSA, such as negative strain rate sensitivity (SRS) [21]. In the present experiments, serrated curves were not observed in the compression tests because of the very short gage length. Nevertheless, the negative SRS that was observed indicated that DSA was taking place.

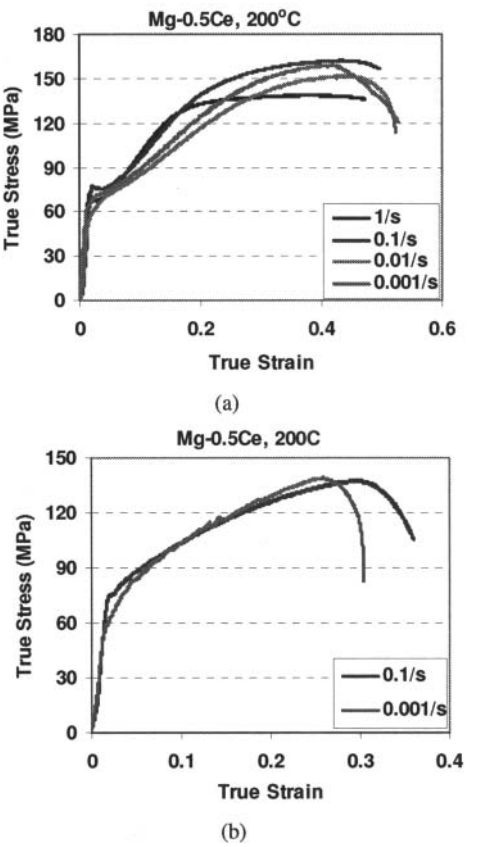

Figure 2. True stress-true strain curves for the (a) compression and (b) tension tests conducted at 200°C at selected strain rates.

During the compression tests, the DSA effects were superimposed on those of twinning and glide. Nevertheless, the higher compression flow stress at 0.001/s than at 0.01/s indicates that the effect of DSA on the flow stress is greater at the lower strain rate. This can be attributed to the solute drag associated with Ce addition being greater at the lower strain rate at 200°C because there is a better match between the Ce diffusivity and the dislocation velocity at that strain rate. The specimens exhibited negative rate sensitivity over the entire strain rate change. Thus DSA can be considered to take place in the strain rate range from 0.001/s to 0.1/s. The occurrence of DSA also led to a decrease in the tensile ductility.

The Ce solute contents of the as-extruded sample and the samples after the different heat treatments were displayed in Table I. As a reference, the equilibrium solubility of Ce in solid magnesium is given in Table II. The fastest cooling rate (about $2.7x10^5$°C/min) employed in treatment H5 led to the highest Ce level (0.16 wt.%), while treatment H3 with the slowest cooling rate (3°C/min) led to the lowest Ce level (0.076wt.%, only half of that in the H5 sample). These observations reveal the importance of cooling rate after extrusion on the solute concentration in Ce-modified alloys.

They show that rapid cooling leads to a supersaturation of Ce at lower temperatures and conversely that minimization of the solute Ce content requires annealing followed by slow cooling.

Table II. The solubility of Ce in solid magnesium at different temperatures [22].

	590 °C	500°C	400 °C	300 °C	200 °C
wt. %	0.74	0.26	0.08	0.06	0.04
at. %	0.13	0.045	0.014	0.010	0.007

The optical microstructures after the various heat treatments are displayed in Figure 3. Compared to the as-extruded material (10μm), the average grain sizes of the heat treated materials have increased into the range 15-25μm. The H3 specimen had the largest average grain size, ~25μm, although its texture was similar to that of the as-extruded sample.

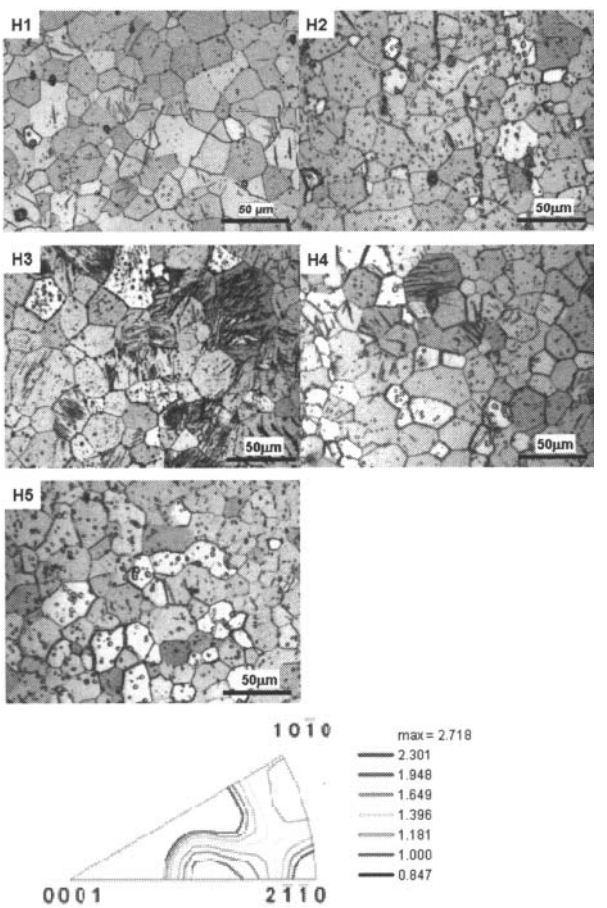

Figure 3. Optical microstructures of the Mg-0.5 wt.% Ce alloy samples after the various heat treatments. The texture of the H3 sample is presented in the inverse pole figure of the extrusion direction, which is vertical in the micrographs.

As shown in Figure 2, a strain rate of 0.001/s led to the lowest strain-to-fracture during compression and to serrated flow curves during tension. It was therefore concluded that the interaction between Ce atoms and dislocations was most pronounced at a strain rate of 0.001/s. To determine whether decreasing the Ce solute content can reduce the detrimental effects of DSA, compression testing was carried out at 200°C/0.001s^{-1} on the samples that had undergone the various heat treatments. The stress-strain curves obtained are presented in Figure 4. Here it can be seen that all the heat-treated specimens had improved ductilities, compared to the as-received material.

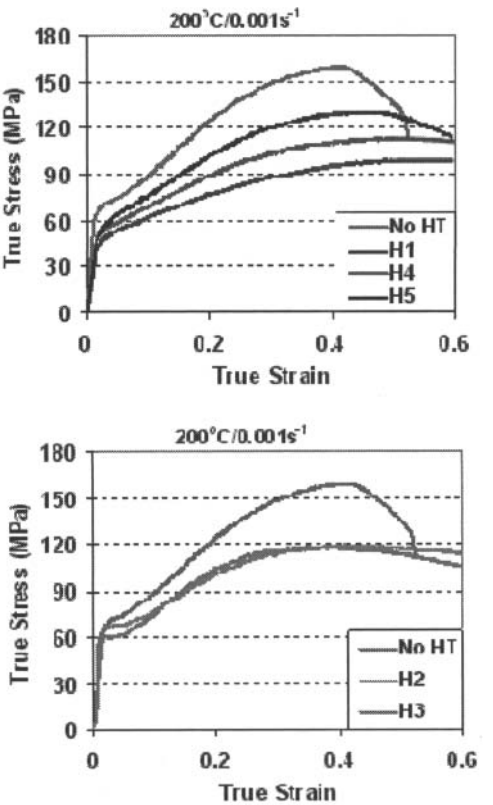

Figure 4. Compression stress-strain curves for the specimens subjected to the different heat treatments.

During heat treatment, the dislocations generated during the extrusion process were annihilated, which reduced the extent of Ce solute/dislocation interaction. Therefore, the H5 specimen did not fracture shortly after reaching peak stress as did the as-extruded sample, although it had the highest Ce solute level (0.16wt.%). Nevertheless, after the peak stress, the load-carrying ability was not maintained over appreciable strains due to the high Ce solute concentration. By contrast, although the H3 specimen had the lowest Ce solute content (0.077wt.%), its flow curve displayed a more marked sigmoidal shape and the lowest strain-to-peak. This is probably because the H3 specimen had a relatively large grain size. In addition, due to the slowest cooling rate, the precipitates in this material were the coarsest and their pinning effect was reduced. The detrimental effect due to DSA appears to have been reduced appreciably in the H1 and H4 specimens during compression. This can also be seen in Figure 5 (a). When the strain rate was increased from 0.001/s to 0.01/s, no negative SRS was observed in the H1 and H3 specimens.

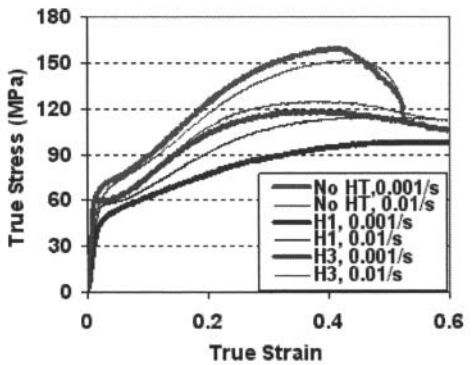

(a)

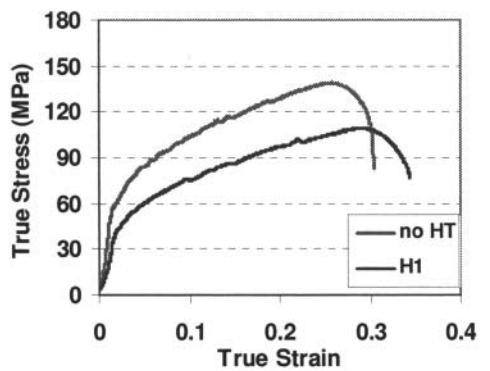

(b)

Figure 5. Stress-strain curves comparison for the specimens undergone different heat treatments during (a) compression at strain rates of 0.01/s and 0.001/s; (b) tension at a strain rate of 0.001/s. All the tests were conducted at 200°C.

However, the H1 specimen still exhibited a serrated flow curve during tension, as displayed in Figure 5(b). This is consistent with the previous observations of Zhu and Nie [13], where their WE54 alloy (Mg-Y-Nd system) exhibited serrated flow even when tested in the peak-aged condition (solution treated at 525°C for 8h and aged at 250°C for 16h). The absence of negative SRS in the compressive H1 samples indicates that annealing reduced the level of solute Ce in those samples and therefore eliminated the DSA effect. This is probably also the reason why the detrimental effect of DSA was essentially absent in the H1 compression sample but not in the tension test.

Conclusions

The effect of solute cerium on the deformation behavior of the Mg-0.5Ce wt.% alloy was investigated at 200°C by means of uniaxial tension and compression tests. At 200°C, DSA took place in the strain rate range from 0.001/s to 0.1/s and was most pronounced at 0.001/s. The occurrence of DSA leads to a decrease in the ductility in both compression and tension. The heat treatment results show that cooling at 25°C/min-50°C/min can significantly reduce the detrimental effect of DSA in compression but not as markedly in tension tests.

Acknowledgments

This research was sponsored by General Motors of Canada and the Natural Sciences and Engineering Research Council of Canada. Discussions with Prof. Matthew Barnett of Deakin University, Australia are gratefully acknowledged.

References

1. R.K. Mishra, et al., "Influence of cerium on the texture and ductility of magnesium extrusions", *Scripta Materialia*, 59 (2008) 562-565.

2. J. Bohlen, et al., "The texture and anisotropy of magnesium-zinc-rare earth alloy sheets", *Acta Materialia*, 55 (2007) 2101-2112.

3. Y. Chino, K. Sassa and M. Mabuchi, "Texture and stretch formability of a rolled Mg-Zn alloy containing dilute content of Y", *Materials Sci. and Eng.: A*, 513-514 (2009) 394-400.

4. J.W. Senn and S.R. Agnew. "Texture randomization of magnesium alloys containing rare earth elements", in the Proceeding of *Magnesium Technology 2008*, TMS, 2008), 153-158.

5. C.J. Ma, et al., "Microstructure and mechanical properties of extruded ZK60 magnesium alloy containing rare earth", *Materials Science and Technology*, 20 (2004) 1661-1665.

6. J. Gröbner and R. Schmid-Fetzer, "Thermodynamic modeling of the Mg-Ce-Gd-Y system", *Scripta Materialia*, 63 (2010) 674-679.

7. N. Stanford, et al., "Effect of Al and Gd Solutes on the Strain Rate Sensitivity of Magnesium Alloys", *Metallurgical and Materials Transactions A*, 41 (2010) 734-743.

8. B.L. Wu, et al., "Ductility enhancement of extruded magnesium via yttrium addition", *Materials Science and Engineering: A*, 527 (2010) 4334-4340.

9. N. Stanford, "Micro-alloying Mg with Y, Ce, Gd and La for texture modification--A comparative study", *Materials Science and Engineering: A*, 527 (2010) 2669-2677.

10. Y.Chino, M. Kado and M. Mabuchi, "Compressive deformation behavior at room temperature–773 K in Mg–0.2 mass% (0.035at.%)Ce alloy", *Acta Mater.*, 56 (2008) 387-394.

11. L. Jiang, et al., "Effect of cerium on the deformation behavior of two Mg-Ce alloys". in the proceeding of *Magnesium Technology 2010*. TMS, 2010), 343-346.

12. S.L. Couling, "Yield points in a dilute magnesium-thorium alloy", *Acta Metallurgica*, 7 (1959) 133-134.

13. L. Gao, R.S. Chen and E.H. Han, "Characterization of dynamic strain ageing in Mg-3.11wt.%Gd alloy", in the proceeding of *Magnesium Technology 2009*. TMS, 2009), 269-272.

14. S.M. Zhu and J.F. Nie, "Serrated flow and tensile properties of a Mg-Y-Nd alloy", *Scripta Materialia*, 50 (2004) 51-55.

15. N. Stanford, "Effect of composition on the texture and deformation behaviour of wrought Mg alloys", *Scripta Materialia*, 58 (2008) 179-182.

16. N. Stanford, A. Beer, C. Davies, M.R. Barnett, "Effect of microalloying with rare-earth elements on the texture of extruded magnesium-based alloys", *Scripta Materialia*, 59 (2008) 772-775.

17. L.W.F. Mackenzie and M.O. Pekguleryuz, "The recrystallization and texture of magnesium-zinc-cerium alloys", *Scripta Materialia*, 59 (2008) 665-668.

18. N. Stanford and M.R. Barnett, "The origin of "rare earth" texture development in extruded Mg-based alloys and its effect on tensile ductility", *Mater. Sci. Eng. A*, 496 (2008) 399-408.

19. A.O. Humphreys, et al., "Warm rolling behaviour of low carbon steels", *Mater. Sci. Tech.*, 19 (2003) 709-714.

20. N. Christodoulou, et al., "Analysis of steady-state thermal creep of Zr-2.5Nb pressure tube material", Metallurgical and Materials Transactions A, 33 (2002) 1103-1115.

21. J.M. Robinson and M.P. Shaw, "Microstructural and mechanical influences on dynamic strain aging phenomena", *International Materials Reviews*, 39 (1994) 113-122.

22. L. Rokhlin, "Dependence of the rare earth metal solubility in solid magnesium on its atomic number", *Journal of Phase Equilibria*, 19 (1998) 142-145.